SAND2010-0048C

Fuel-Structure Dependence of Benzene Formation Processes in Premixed Flames Fueled by C_6H_{12} Isomers

N. Hansen,[a)*] T. Kasper,[a)†] B. Yang,[b)] T. A. Cool,[b)] W. Li,[c)] P. R. Westmoreland,[c)]

P. Oßwald,[d)] K. Kohse-Höinghaus[d)]

[a)] *Combustion Research Facility, Sandia National Laboratories, Livermore, CA 94551, USA*

[b)] *School of Applied and Engineering Physics, Cornell University, Ithaca, NY 14853, USA*

[c)] *Department of Chemical and Biomolecular Engineering, North Carolina State University, Raleigh, NC 27695, USA*

[d)] *Department of Chemistry, Bielefeld University, D-33615 Bielefeld, Germany*

to be submitted to:

33rd International Symposium on Combustion
"Soot, PAH and Other Large Molecules" Colloquium

Word Count (MS Word)

Abstract:	153
Introduction:	406
Experimental Procedures:	411
Results and Discussion:	2574
Conclusions:	233
Acknowledgements:	66
42 References:	769
5 Figures: 123+162+162+440+441	1328
Total Words:	**5785**

* Corresponding author:
Email: nhansen@sandia.gov; Fax: 925-294-2276; Tel.: 925-294-6272
† Current address: SRI International, Menlo Park, CA 94025-3493, USA

Abstract

The fuel-structure dependent significance of various benzene formation pathways is analyzed using data from rich (ϕ=1.7) flames fueled by four C_6H_{12} isomers: 1-hexene, cyclohexane, methylcyclopentane, and 3,3-dimethyl-1-butene. The isomer-resolved chemical compositions of the four premixed, laminar low-pressure flat flames are determined by flame-sampling molecular-beam mass spectrometry employing single-photon ionization by synchrotron generated vacuum-ultraviolet photons. Isomer-resolving photoionization efficiency curves and quantitative mole fraction profiles reveal the dominant fuel destruction pathways, the influence of different fuel consumption processes on the formation of commonly considered benzene precursors, and the contributions of several routes towards benzene formation. While propargyl and allyl radicals dominate benzene formation in the combustion of 1-hexene, contributions from reactions involving *i*-C_4H_5 and C_5H_5 radicals are revealed in the flames of 3,3-dimethyl-1-butene and methylcyclopentane, respectively. Close to the burner surface, successive dehydrogenation of the fuel is found to be important for the cyclohexane flame and to some smaller extent for the methylcyclopentane flame.

Keywords

C_6H_{12} fuels, laminar flames, mass spectrometry, benzene formation

1. Introduction

A detailed description of the complex chemistry involved in the formation of polycyclic aromatic hydrocarbons (PAH's) and soot particles in combustion environments remains an intriguing problem. Over the past few years, pathways leading to benzene as the "first aromatic ring" have received considerable interest in the combustion community. These processes are believed to be the first step in the overall course of PAH and soot formation and to determine the generation of these air pollutants. It is now well accepted that aromatic species are produced in flames by a variety of reactions, most of which include resonantly stabilized radicals like C_3H_3, C_3H_5, *i*-C_4H_5, and *c*-C_5H_5 [1-4]. In many fuel-rich hydrocarbon flames, the propargyl+propargyl reaction seems to be the dominant pathway to benzene (or to phenyl+H) [2-3]. However, other pathways may contribute as well, with their significance depending largely on the chemical structure of the fuel [5-9].

The aim of this experimental study is to elucidate the importance of benzene formation routes in flames fueled by the following isomeric C_6H_{12} compounds: 1-hexene (1HX), cyclohexane (CHX), methylcyclopentane (MCP), and 3,3-dimethyl-1-butene (DMB). The chemical structures of these four isomeric compounds are shown in Fig. 1. We investigate the effects of the chemical structure of the fuels on the processes of fuel consumption and aromatics formation by comparing flame-sampled molecular-beam mass spectrometric data from fuel-rich laminar premixed $C_6H_{12}/O_2/Ar$ flames with each other and with literature flame data.

The combustion chemistries of these fuels are of interest for several reasons. Alkenes, cycloalkanes, and methylcycloalkanes are present in commercial fuels, with CHX being an especially important constituent of the new generation of fuels derived from tar sands and oil shales [9-11]. Chemically, the C_6H_{12} isomers selected for this study represent a variety of

structures, including long-chain and branched alkenes and cycloalkanes and their methyl-substituted derivatives. The main structural features of 1HX and DMB are allylic bonds that are much weaker than their alkyl analogues [3]. Breaking of these weak C-C bonds, leads to the formation of C_3 and C_4 benzene precursors [11-15]. An interesting feature of the chemistry of the CHX and MCP fuels is the competition between the dehydrogenation routes and the ring-opening with subsequent decomposition to smaller components [9-10, 15-19]. Quantitative mole fractions of benzene and its relevant precursors are thus determined under identical flame conditions for these fuels to understand potential differences with respect to one of the most important steps in molecular-weight growth processes in flames.

2. Experimental Procedures

Premixed laminar $C_6H_{12}/O_2/Ar$ flames, which are fueled by one of the four isomers 1HX, CHX, MCP, or DMB, are stabilized on a water-cooled stainless-steel McKenna burner at a low-pressure of p=30 Torr (40 mbar). The cold-gas composition of the four fuel-rich (ϕ=1.7) flames is uniformly: 30.0% Ar, 58.9% O_2, 11.1% C_6H_{12}. The cold-gas velocity is v=49.2 cm/s at 298 K. The gas flows are controlled with calibrated mass flow controllers and the liquid fuels are metered by a syringe pump, evaporated, and added into the oxidizer stream.

The chemical composition of each flame is analyzed using isomer-resolving flame-sampling molecular-beam mass spectrometry [20]. The experiments, which are performed at the Advanced Light Source of the Lawrence Berkeley National Laboratory, and the data analysis procedures are described in detail elsewhere [4, 20-23]; only a short description is provided here. Gases sampled from the burner-stabilized flat flames are expanded through a quartz nozzle (d~0.4 mm) to a pressure of $p\sim10^{-4}$ Torr. In a second-stage expansion through a conical skimmer,

the molecular beam enters the ionization region ($p \sim 10^{-6}$ Torr) where the flame species are ionized using single-photon ionization. The resulting ions are subsequently separated by their mass-to-charge ratio using a linear time-of-flight mass spectrometer with a resolution of $m/\Delta m \sim 500$ and a detection limit of ~10 ppm [20].

Mass spectra are collected as a function of the distance from the burner (burner scan) and as a function of the photon energy at a fixed distance (energy scan). Mass signals are integrated and corrected for the photon current, fragmentation, and overlapping isotopic contributions. While the burner scans are analyzed to generate profiles of quantitative mole fraction *vs.* distance from burner, the energy scans allow the identification of the isomeric composition of various combustion intermediates via their characteristic photoionization efficiency curves [4]. Mole fraction profiles are obtained for all four flames for more than 40 species with ion masses ranging from 2 (H_2) to 84 (C_6H_{12}). However, only a few critical aspects of the chemical compositions of the flames are discussed here; the complete dataset is available upon request.

The error bars on the mole fraction for some intermediates can be as large as a factor of four, especially if the absolute photoionization cross section is unknown. However, the relative comparisons of the mole fractions, profile shapes, and positions between flames within this study have much smaller uncertainties of about 30%, considering that the experimental and analysis procedures are the same for all four flames.

3. Results and Discussion

3.1. Benzene Mole Fraction Profiles

In previous studies, we have shown that the analysis of the chemical compositions of flames fueled by structural isomers is a suitable approach to elucidate fuel-specific reaction

pathways [23-27]. When established with the same flow conditions, flames fueled by different isomers exhibit a very similar overall combustion characteristic, that is, the temperature profiles and the major species (fuel, H_2, H_2O, CO, O_2, CO_2, and Ar) mole fraction profiles are identical within the error limits. Differences between the flames in the chemical composition of other species are thus due to the structural differences of the fuel compounds and their differences in initial fuel destruction reactions.

For all four flames studied here, the mole fractions of benzene as a function of distance to the burner are shown in Fig. 2. The following differences are immediately visible: (i) The maximum mole fractions of benzene are larger in the MCP and CHX flames than in the flames fueled by the alkene isomers 1HX and DMB. (ii) The mole fraction of benzene is the smallest in the 1HX flame. (iii) The shape of the benzene mole fraction profile is different for the CHX flame, in which significant amounts of benzene are formed close to the burner. A similar behavior can be seen in the MCP flame to a much smaller extent.

It is apparent that the presence of a five- or six-membered ring structure in the fuel compound promotes the formation of benzene. The heights and shapes of the benzene mole fraction profiles in the CHX and MCP flames are in principal accordance with proposed reaction mechanisms, in which C_5 and C_6 ring structures are converted to benzene by rapid ring-enlargement reactions and successive dehydrogenation [3, 5, 8-9, 28].

3.2. Fuel Consumption Pathways

For a more detailed analysis of different benzene formation pathways, it is essential to consider fuel-consumption processes and their influence on the formation of common benzene precursors. Flames are highly reactive systems in which a vast number of fuel decomposition

reactions can occur, including H-atom abstraction and simple and complex bond fissions [3]. For the four flames studied here, their different peak mole fractions (Fig. 3) and photoionization efficiency curves (Fig. 4) reveal several important fuel consumption pathways; the details of which are discussed in this Section.

For 1HX, the following decomposition reactions are likely to occur [11, 13-14]:

$$CH_2=CH\text{-}CH_2\text{-}CH_2\text{-}CH_2\text{-}CH_3 \rightleftarrows CH_2=CH\text{-}CH_2\bullet + \bullet CH_2\text{-}CH_2\text{-}CH_3 \quad \text{(R1)}$$

$$CH_2=CH\text{-}CH_2\text{-}CH_2\text{-}CH_2\text{-}CH_3 + X\ (H, O, OH) \rightleftarrows CH_2=CH\text{-}CH\bullet\text{-}CH_2\text{-}CH_2\text{-}CH_3 + HX \quad \text{(R2)}$$

$$CH_2=CH\text{-}CH_2\text{-}CH_2\text{-}CH_2\text{-}CH_3 \rightleftarrows CH_2=CH\text{-}CH_3 + CH_2=CH\text{-}CH_3 \quad \text{(R3)}$$

For resonantly stabilized radicals like $CH_2=CH\text{-}CH_2\bullet$ (allyl) or $CH_2=CH\text{-}CH\bullet\text{-}CH_2\text{-}CH_2\text{-}CH_3$ (3-hexenyl) only one resonance structure will mostly be shown. Abstraction of an alkyl H-atom and fission of an alkyl C-C bond are further reaction options; however, their rates are much slower than the abstraction and fission of the respective allylic bonds. The initially formed radicals are subsequently consumed dominantly by β-scissions [3]:

$$CH_2=CH\text{-}CH\bullet\text{-}CH_2\text{-}CH_2\text{-}CH_3 \rightleftarrows CH_2=CH\text{-}CH=CH_2 + \bullet CH_2\text{-}CH_3 \quad \text{(R4)}$$

$$CH_2=CH\text{-}CH\bullet\text{-}CH_2\text{-}CH_2\text{-}CH_3 \rightleftarrows CH_2=CH\text{-}CH=CH\text{-}CH_2\text{-}CH_3 + H \quad \text{(R5)}$$

Since C-C bonds are much weaker than C-H bonds, dissociation to 1,3-butadiene (R4) is preferred; the possible formation of $CH_2=C=CH\text{-}CH_2\text{-}CH_2\text{-}CH_3$ is energetically not favored. The dominant decomposition of 1HX into C_3 and C_4 species can be seen in Fig. 3 in which the maximum mole fractions of C_3H_5, C_3H_6, C_4H_6, and C_5H_6 are combined for all four flames. The 1HX flame produces by far the largest amounts of allyl and propene, while the production of C_4H_6 is only larger in the equivalent cyclohexane flame (which will be discussed later). Further evidence for these fuel decomposition channels are shown in Figs. 4(a) and (b) in which the

flame-sampled photoionization efficiency (PIE) curves of *m/z*=42 (CH_2CO and C_3H_6) and *m/z*=54 (C_4H_6) are shown together with PIE curves of propene, ketene, 1,3-butadiene, 1,2-butadiene, and 2-butyne. Compared with the DMB flame, which produces less C_3 species, the *m/z*=42 signal from the 1HX flame is dominated by propene. Figure 4(b) shows that signal at *m/z*=54 originates indeed from 1,3-butadiene, which is likely to be formed directly from the fuel through R2 and R4.

Similarly to 1-hexene, DMB possesses an allylic C-C bond; thus, the unimolecular dissociation of DMB into methyl and dimethylallyl (2-methylbut3-en-2-yl) is a possible decomposition pathway:

$$CH_2=CH\text{-}C(CH_3)_3 \rightleftarrows CH_2=CH\text{-}C\bullet(CH_3)_2 + \bullet CH_3 \quad \text{(R6)}$$

However, DMB does not have any allylic C-H bonds. H-Abstraction reactions, which are likely to occur on the methyl groups, result in a non-resonantly stabilized radical:

$$CH_2=CH\text{-}C(CH_3)_3 + X\ (H, O, \text{and } OH) \rightleftarrows CH_2=CH\text{-}C(CH_3)_2CH_2\bullet + HX \quad \text{(R7)}$$

The fuel consumption process through H-abstraction reaction at the CH_2 group, which is likely to lead to acetylene and *t*-butyl radicals, is expected to be overall slower than for R7 as the H-abstraction at the methyl groups can occur more frequently. The initially produced radicals in R6 and R7 $CH_2=CH\text{-}C\bullet(CH_3)_2$ and $CH_2=CH\text{-}C(CH_3)_2CH_2\bullet$ can further undergo β-scissions:

$$CH_2=CH\text{-}C\bullet(CH_3)_2 \text{ or } CH_2=CH\text{-}C(CH_3)_2CH_2\bullet \rightleftarrows CH_2=CH\text{-}C(CH_3)=CH_2 + H \text{ or } \bullet CH_3 \quad \text{(R8)}$$

$$CH_2=CH\text{-}C\bullet(CH_3)_2 \rightleftarrows CH_2=C=C(CH_3)_2 + H \quad \text{(R9)}$$

The presence of 2-methyl-1,3-butadiene ($CH_2=CH\text{-}C(CH_3)=CH_2$) in the DMB flame is verified by the comparison of the flame-sampled PIE curve for *m/z*=68 (C_5H_8), which is shown in Fig. 4(c), with the ionization energies of various C_5H_8 isomers [29-30]. As indicated by vertical

arrows in Fig. 4(c), the experimentally observed ionization threshold of 8.87±0.05 eV is in good agreement with the known ionization energy of CH_2=CH-C(CH_3)=CH_2 [29]. The PIE curve of 2-methyl-1,3-butadiene is currently unknown, so that the presence of isomers with larger ionization energies, including CH_2=C=C(CH_3)$_2$, cannot be verified unambiguously.

Both of the closed-shell products in R8 and R9 feature weak allylic C-C bonds, and by breaking them, two isomeric C_4H_5 radicals can be formed: *i*-C_4H_5 (CH_2=CH-C•=CH_2 ↔ •CH_2-CH=C=CH_2) and methylallenyl (CH_2=C=C•-CH_3 ↔ •CH_2-C≡C-CH_3). The recombination reactions of these radicals with H atoms lead to 1,2- and 1,3-butadiene and 2-butyne. Evidence for the decomposition of DMB to C_4 species is found in the pronounced maximum mole fraction of C_4H_6 in the DMB flame and in the flame-sampled PIE curve for *m/z*=54 (C_4H_6), which can only be reproduced by a weighted sum of PIE's from 1,2- and 1,3-butadiene and 2-butyne, see Figs. (3) and (4b), respectively.

CHX and MCP do not have allylic C-H or C-C bonds; they are most likely consumed by H-abstraction reactions forming the cyclohexyl radical (*c*-C_6H_{11}) and any of the four isomeric five-membered ring C_6H_{11} radicals [9, 31]:

$$c\text{-}C_6H_{12} + X\ (H, O, OH) \rightleftarrows c\text{-}C_6H_{11}\bullet + HX \qquad (R10)$$

$$c\text{-}C_5H_9\text{-}CH_3 + X\ (H, O, OH) \rightleftarrows c\text{-}C_5H_8\bullet\text{-}CH_3\ (\text{or } c\text{-}C_5H_9\text{-}CH_2\bullet) + HX \qquad (R11)$$

The isomerization reactions between CHX and 1HX and between MCP and linear and branched C_6H_{12} isomers seem to be of limited importance in the radical-rich environment of flames [9]; this is also true for the C-C bond fission in MCP to form methyl and cyclopentyl radicals [32]. Again, the initially formed radicals can undergo fast β-scissions; that is, cyclohexyl radicals

undergo a ring-opening process to form 6-hexenyl (CH_2=CH-CH_2-CH_2-CH_2-CH_2•) radicals (preferred) or a simple C-H bond fission to form cyclohexene:

$$c\text{-}C_6H_{11} \rightleftarrows CH_2\text{=}CH\text{-}CH_2\text{-}CH_2\text{-}CH_2\text{-}CH_2\bullet \text{ (or } c\text{-}C_6H_{10} + H) \quad \text{(R12)}$$

While cyclohexene can undergo further dehydrogenation processes to eventually form benzene [8-9], the 6-hexenyl radical is largely consumed by subsequent β-scissions and isomerization:

$$CH_2\text{=}CH\text{-}CH_2\text{-}CH_2\text{-}CH_2\text{-}CH_2\bullet \rightleftarrows CH_2\text{=}CH\text{-}CH_2\text{-}CH_2\bullet + CH_2\text{=}CH_2 \quad \text{(R13)}$$

$$CH_2\text{=}CH\text{-}CH_2\text{-}CH_2\bullet \rightleftarrows CH_2\text{=}CH\text{-}CH\text{=}CH_2 + H \text{ (or } CH_2\text{=}CH\bullet + C_2H_4) \quad \text{(R14)}$$

$$CH_2\text{=}CH\text{-}CH_2\text{-}CH_2\text{-}CH_2\text{-}CH_2\bullet \rightleftarrows CH_2\text{=}CH\text{-}CH\bullet\text{-}CH_2\text{-}CH_2\text{-}CH_3 \quad \text{(R15)}$$

The 3-hexenyl radical then decomposes according to R4 and R5. The dominance of the CHX consumption through C_4 species manifests itself in the maximum mole fraction of C_4H_6 (Fig. 3), which exceeds the mole fractions in the other flames by about a factor of 2 or more. Further evidence is shown in the flame-sampled PIE curve for *m/z*=54 (C_4H_6), which is clearly dominated by the presence of 1,3-butadiene, see Fig. 4(b).

For the MCP flame, the initially formed isomeric *c*-C_5H_8•-CH_3 (or *c*-C_5H_9-CH_2•) radicals decompose by β-scission through C-C (preferred) or C-H bond rapture. The large number of conceivable products makes it currently unfeasible to assign isomeric structures to the radical and closed-shell products. However, under typical combustion conditions, the C_5 ring should initially remain intact and the formation of cyclopentene and methyl should be dominant [33]. As shown in Fig. 4(c), cyclopentene is easily identified by its ionization energy and photoionization efficiency curve, as is 1,3-pentadiene, a product from cyclopentene isomerization. The larger presence of cyclic C_5 species in the MCP flame compared with the other flames is evident in Fig. 3.

3.3. Benzene Formation Pathways

From the discussion of the isomer-specific fuel decomposition processes it is obvious that within the four C_6H_{12} flames, the formation of the commonly considered benzene precursors C_3H_3, C_3H_5, *i*-C_4H_5, and C_5H_5 is influenced by the chemical structure of the fuel. Therefore, it is likely that the fuel structure has an influence on the importance of various benzene formation routes. Although the four C_6H_{12} flames await detailed flame chemistry modeling, the results presented here can be inferred from the experimental data and comparison to literature data from similar flames: acetylene (ϕ=2.25 [34] and 2.4 [35]), ethylene (ϕ=1.9 [36]), allene (ϕ=1.0 [24] and 1.8 [25]), propyne (ϕ=1.0 [24] and 1.8 [25]), propene (ϕ=1.5 [26] and 2.3 [37]), propane (ϕ=1.8 [21]), 1,3-butadiene (ϕ=1.8 [6] and 2.4 [38]), cyclopentene (ϕ=2.0 [7]), and cyclohexane (ϕ=1.0 [8]). For all these flames, the conditions, i.e. flow rate, pressure, Ar mole fraction, and maximum flame temperature, are generously comparable; with the exception of the ϕ=2.4 1,3-butadiene flame [38], which is diluted by only 3% Ar.

In the 1HX flame, the fuel decomposes dominantly to C_3 species (see Section 3.2.) and therefore it seems plausible that benzene formation is dominated by the corresponding C_3+C_3 chemistry, i.e. the propargyl+propargyl or propargyl+allyl reaction, both of which are commonly proposed cyclization steps [39-40]. While large amounts of allyl are formed directly through R1, propargyl radicals are likely to be formed by subsequent H-abstraction reactions. Our finding that C_3+C_3 reactions are likely to dominate benzene formation in the 1HX flame is in disagreement with the work of Yahyaoui *et al.* [11]. They found that in jet-stirred reactor and shock tube studies benzene is formed from 1HX through the reversed R12 and subsequent dehydrogenation of the cyclohexyl radical. In the 1HX flame, the reactions of C_4 and C_5 species

should not contribute significantly to benzene formation. Nevertheless, the larger amounts of C_4 fragments, may lead to small contributions from *i*-C_4H_5+C_2H_2 [41]. However, the reaction

$$i\text{-}C_4H_5 + H \rightleftarrows C_3H_3 + CH_3, \qquad \text{(R16)}$$

is expected to be fast, thus limiting the contribution of *i*-C_4H_5+C_2H_2 to benzene formation in favor of the C_3H_3+C_3H_3 recombination [6]. Consequently, the amount of benzene formed in the 1HX flame, which is the smallest in the four flames studied here, can be interpreted as an upper limit on how much benzene can be formed through C_3+C_3 reactions in this set of flames.

To emphasize this argument, we correlate the maximum mole fractions of benzene in the four C_6H_{12} flames and the above mentioned literature flames to the observed maximum mole fractions of C_3H_3. The corresponding C_6H_6 *vs.* C_3H_3 plot in Fig. 5(a) reveals the following: (i) With the exception of the rich 1,3-butadiene flame (ϕ=2.4), for a given propargyl mole fraction, fuels containing a ring structure produce larger amounts of benzene, thus indicating direct routes via dehydrogenation and ring-enlargement reactions as discussed in Section 3.1. (see also Fig. 2). (ii) For non-cyclic fuels, the maximum levels of benzene seem to be close to or below the dotted line; again with the exception of the 1,3-butadiene flame (ϕ=2.4). (iii) The maximum mole fractions of the propargyl radical in the 1HX, CHX, MCP, and DMB flames studied here are almost identical. That is, the different benzene levels encountered in the C_6H_{12} flames (Fig. 2) cannot be explained by the differences in mole fractions of propargyl, and additional pathways are likely to contribute in the CHX, MCP, and DMB flames.

One of these conceivable pathways is the reaction of *i*-C_4H_5 with C_2H_2 [41]. This reaction is an important cyclization reaction in flames, in which *i*-C_4H_5 is formed directly from the fuel, i.e. 1,3-butadiene [6]. In the CHX and DMB flames, 1,3-butadiene and *i*-C_4H_5 are identified as possible fuel-decomposition products; thus, it seems likely that the *i*-C_4H_5+C_2H_2 reaction

contributes to the ring formation process in these flames. However, we keep in mind that R16 tends to limit the contribution of *i*-C_4H_5 radical reactions. The observed maximum mole fractions of C_4H_5 from the C_6H_{12} flames and from the literature flames are presented in Fig. 5(b) in a C_6H_6 *vs.* C_4H_5 correlation plot. Although the older literature flame data do not distinguish between various C_4H_5 isomers, based on Ref. [42] the presence of the resonantly stabilized *i*-C_4H_5 radical can be assumed. For most flames considered here, C_4H_5 mole fractions are below 10^{-4}. For these flames, no correlation is seen between the reported maximum mole fractions of C_4H_5 and benzene. That is, the large differences in the level of benzene cannot be explained by the changes in C_4H_5 mole fractions; with the exception of the fuel-rich CHX flame, contributions of C_4H_5 reactions towards benzene formation are likely to be negligible within those flames. Significant amounts of C_4H_5 are only observed when using DMB or 1,3-butadiene as a fuel. For these flames, a correlation is seen between the C_4H_5 and benzene mole fractions as indicated by the dotted line in Fig. 5(b): larger mole fractions of C_4H_5 lead to larger mole fractions of benzene. Having established that *i*-C_4H_5+C_2H_2 accounts significantly for aromatics formation in 1,3-butadiene flames [6], the levels of C_4H_5 and the correlation as shown in Fig. 5(b) may indicate that this reaction adds to the benzene levels in the rich DMB flame.

Another pathway conceivably contributing towards benzene formation is the reaction of resonantly stabilized cyclopentadienyl (C_5H_5) with methyl radicals [3]. The corresponding C_6H_6 *vs.* C_5H_5 correlation plot, which includes available data from the four C_6H_{12} flames and the literature, is shown in Fig. 5(c). For most flames, the mole fractions of C_5H_5 are close to or below 10^{-4} and they cannot explain the observed large differences of the benzene mole fractions. Therefore, it can be concluded that reactions of C_5H_5 are not of immediate importance for benzene formation under these conditions. Only the flames fueled by MCP and cyclopentene

(Ref. [7]) produce C_5H_5 in significant amounts, and indeed, these are the flames producing the largest amounts of benzene. A linear correlation between mole fractions of C_6H_6 and C_5H_5 can be seen as indicated by the dotted line in Fig. 5(c). It is worth mentioning that at typical flat-flame conditions, C_5H_5 radicals tend to dissociate into C_3H_3+C_2H_2, thus limiting the importance of C_5H_5 radical reactions. However, since the observed levels of C_3H_3 and C_4H_5 cannot explain the higher levels of benzene in the MCP flame, it seems likely that resonantly stabilized C_5H_5 radicals play a significant role in benzene formation in this flame, in which it is readily (directly) formed from the fuel.

The last pathway to benzene, which shall be discussed in this paper, is successive dehydrogenation of the fuel. As pointed out in Section 3.1., larger amounts of benzene are formed in the CHX flame close to the burner, indicating that the dehydrogenation route is important close to the burner. This pathway was found to be the dominant benzene formation pathway in a stoichiometric CHX flame [8-9] and is likely to contribute also in the fuel-rich flame studied here. The early formation of benzene is also observed, although to a smaller degree, in the MCP flame, thus indicating a similar dehydrogenation mechanism. The initially formed fulvene can subsequently be transformed into benzene by an H-assisted isomerization reaction [41].

4. Conclusions

This study expands our previous work on the combustion chemistry of smaller C_3-C_5 hydrocarbons [6-7, 24-25, 30, 42] towards the chemistry of larger, more structurally complex hydrocarbons that are contained in all liquid fuels. Low-pressure premixed laminar flames (ϕ=1.7) fueled by one of the four C_6H_{12} isomers 1-hexene, cyclohexane, methylcylopentane, and

3,3-dimethyl-1-butene are analyzed by flame-sampling molecular-beam mass spectrometry employing isomer-resolving single-photon VUV ionization. Various mole fraction profiles and isomer-specific fuel consumption pathways are discussed with an emphasis on fuel decomposition processes and the formation of benzene and its precursors.

From the comparison of the photoionization efficiency curves and the mole fraction profiles from the four C_6H_{12} flames with each other and with literature flame data, we conclude that benzene is formed by different pathways depending on the structure of the fuel. In the flames fueled by the linear (1HX) and branched alkenes (DMB), the C_3+C_3 type reactions dominate the benzene formation. The *i*-C_4H_5+C_2H_2 reaction is likely to contribute to the overall benzene formation in the DMB and CHX flames. Reactions of C_5H_5 are found not to be important in the 1HX and DMB flames, however they contribute to the benzene level in the MCP flame in which C_5H_5 can be directly formed from the fuel. Successive dehydrogenation of the fuel is found to contribute to benzene formation close to the burner in the MCP flame and in the CHX flame.

Acknowledgement

We thank Paul Fugazzi and Sarah Ferrell for technical assistance. This work is supported by the Office of Basic Energy Sciences (BES), U.S. Department of Energy (USDOE), under DE-FG02-91ER14192 (PRW) and DE-FG02-01ER1518 (TAC), and by the DFG under KO 1363/18-3 (KKH). Sandia is a multi-program laboratory operated by Sandia Corporation for NNSA under contract DE-AC04-94-AL85000. The Advanced Light Source is supported by BES/USDOE under DE-AC02-05CH11231.

References:

[1] H. Richter, J. B. Howard, *Prog. Energy Combust. Sci.* 26 (4-6) (2000) 565-608.

[2] J. A. Miller, M. J. Pilling, J. Troe, *Proc. Combust. Inst.* 30 (1) (2005) 43-88.

[3] C. S. McEnally, L. D. Pfefferle, B. Atakan, K. Kohse-Höinghaus, *Prog. Energy Combust. Sci.* 32 (3) (2006) 247-294.

[4] N. Hansen, T. A. Cool, P. R. Westmoreland, K. Kohse-Höinghaus, *Prog. Energy Combust. Sci.* 35 (2) (2009) 168-191.

[5] H. R. Zhang, E. G. Eddings, A. F. Sarofim, C. K. Westbrook, *Proc. Combust. Inst.* 32 (1) (2009) 377-385.

[6] N. Hansen, J. A. Miller, T. Kasper, K. Kohse-Höinghaus, P. R. Westmoreland, J. Wang, T. A. Cool, *Proc. Combust. Inst.* 32 (1) (2009) 623-630.

[7] N. Hansen, T. Kasper, S. J. Klippenstein, P. R. Westmoreland, M. E. Law, C. A. Taatjes, K. Kohse-Höinghaus, J. Wang, T. A. Cool, *J. Phys. Chem. A* 111 (19) (2007) 4081-4092.

[8] M. E. Law, P. R. Westmoreland, T. A. Cool, J. Wang, N. Hansen, C. A. Taatjes, T. Kasper, *Proc. Combust. Inst.* 31 (1) (2007) 565-573.

[9] H. R. Zhang, L. K. Huynh, N. Kungwan, Z. Yang, S. Zhang, *J. Phys. Chem. A* 111 (19) (2007) 4102-4115.

[10] E. J. Silke, W. J. Pitz, C. K. Westbrook, M. Ribaucour, *J. Phys. Chem. A* 111 (19) (2007) 3761-3775.

[11] M. Yahyaoui, N. Djebaili-Chaumeix, P. Dagaut, C. E. Paillard, S. Gail, *Combust. Flame* 147 (1-2) (2006) 67-78.

[12] M. Yahyaoui, N. Djebaili-Chaumeix, C.-E. Paillard, S. Touchard, R. Fournet, P. A. Glaude, F. Battin-Leclerc, *Proc. Combust. Inst.* 30 (1) (2005) 1137-1145.

[13] C. S. McEnally, L. D. Pfefferle, *Combust. Flame* 143 (3) (2005) 246-263.

[14] M. Mehl, G. Vanhove, W. J. Pitz, E. Ranzi, *Combust. Flame* 155 (4) (2008) 756-772.

[15] J. H. Kiefer, K. S. Gupte, L. B. Harding, S. J. Klippenstein, *J. Phys. Chem. A* 113 (48) (2009) 13570-13583.

[16] D. Voisin, A. Marchal, M. Reuillon, J.-C. Boettner, *Combust. Sci. Tech.* 138 (1-6) (1998) 137-158.

[17] C. S. McEnally, L. D. Pfefferle, *Combust. Flame* 136 (1-2) (2004) 155-167.

[18] F. Buda, B. Heyberger, R. Fournet, P. A. Glaude, V. Warth, F. Battin-Leclerc, *Energy Fuels* 20 (4) (2006) 1450-1459.

[19] B. Sirjean, F. Buda, H. Hakka, P. A. Glaude, R. Fournet, V. Warth, F. Battin-Leclerc, M. Ruiz-Lopez, *Proc. Combust. Inst.* 31 (1) (2007) 277-284.

[20] T. A. Cool, A. McIlroy, F. Qi, P. R. Westmoreland, L. Poisson, D. S. Peterka, M. Ahmed, *Rev. Sci. Instrum.* 76 (9) (2005) 094102.

[21] T. A. Cool, K. Nakajima, C. A. Taatjes, A. McIlroy, P. R. Westmoreland, M. E. Law, A. Morel, *Proc. Combust. Inst.* 30 (1) (2005) 1681-1688.

[22] C. A. Taatjes, N. Hansen, D. L. Osborn, K. Kohse-Höinghaus, T. A. Cool, P. R. Westmoreland, *Phys. Chem. Chem. Phys.* 10 (1) (2008) 20-34.

[23] P. Osswald, U. Struckmeier, T. Kasper, K. Kohse-Höinghaus, J. Wang, T. A. Cool, N. Hansen, P. R. Westmoreland, *J. Phys. Chem. A* 111 (19) (2007) 4093-4103.

[24] N. Hansen, J. A. Miller, P. R. Westmoreland, T. Kasper, K. Kohse-Höinghaus, J. Wang, T. A. Cool, *Combust. Flame* 156 (11) (2009) 2153-2164.

[25] N. Hansen, J. A. Miller, C. A. Taatjes, J. Wang, T. A. Cool, M. E. Law, P. R. Westmoreland, *Proc. Combust. Inst.* 31 (1) (2007) 1157-1164.

[26] J. Wang, U. Struckmeier, B. Yang, T. A. Cool, P. Osswald, K. Kohse-Höinghaus, T. Kasper, N. Hansen, P. R. Westmoreland, *J. Phys. Chem. A* 112 (39) (2008) 9255-9265.

[27] C. K. Westbrook, W. J. Pitz, P. R. Westmoreland, F. L. Dryer, M. Chaos, P. Osswald, K. Kohse-Höinghaus, T. A. Cool, J. Wang, B. Yang, N. Hansen, T. Kasper, *Proc. Combust. Inst.* 32 (1) (2009) 221-228.

[28] L. V. Moskaleva, A. M. Mebel, M. C. Lin, *Proc. Combust. Inst.* 26 (1) (1996) 521-526.

[29] G. Bieri, F. Burger, E. Heilbronner, J. P. Maier, *Helv. Chem. Acta* 60 (7) (1977) 2213-2233.

[30] N. Hansen, S. J. Klippenstein, J. A. Miller, J. Wang, T. A. Cool, M. E. Law, P. R. Westmoreland, T. Kasper, K. Kohse-Höinghaus, *J. Phys. Chem. A* 110 (13) (2006) 4376-4388.

[31] Y. Yang, A. L. Boehman, *Combust. Flame* in press (2010) doi:10.1016/j.combustflame.2009.08.011.

[32] T. C. Brown, K. D. King, *Int. J. Chem. Kin.* 21 (4) (1989) 251-266.

[33] B. Sirjean, P. A. Glaude, M. Ruiz-Lopez, R. Fournet, *J. Phys. Chem. A* 112 (46) (2008) 11598-11610.

[34] Y. Li, L. Zhang, Z. Tian, T. Yuan, K. Zhang, B. Yang, F. Qi, *Proc. Combust. Inst.* 32 (1) (2009) 1293-1300.

[35] P. R. Westmoreland, J. B. Howard, J. P. Longwell, *Proc. Combust. Inst.* 21 (1) (1986) 773-782.

[36] A. Bhargava, P. R. Westmoreland, *Combust. Flame* 113 (3) (1998) 333-347.

[37] B. Atakan, A. T. Hartlieb, J. Brand, K. Kohse-Höinghaus, *Proc. Combust. Inst.* 27 (1) (1998) 435-444.

[38] J. A. Cole, J. D. Bittner, J. P. Longwell, J. B. Howard, *Combust. Flame* 56 (1) (1984) 51-70.

[39] Y. Georgievskii, J. A. Miller, S. J. Klippenstein, *Phys. Chem. Chem. Phys.* 9 (31) (2007) 4259-4268.

[40] C. J. Pope, J. A. Miller, *Proc. Combust. Inst.* 28 (2) (2000) 1519-1527.

[41] J. P. Senosiain, J. A. Miller, *J. Phys. Chem. A* 111 (19) (2007) 3740-3747.

[42] N. Hansen, S. J. Klippenstein, C. A. Taatjes, J. A. Miller, J. Wang, T. A. Cool, B. Yang, R. Yang, L. X. Wei, C. Q. Huang, J. Wang, F. Qi, M. E. Law, P. R. Westmoreland, *J. Phys. Chem. A* 110 (10) (2006) 3670-3678.

Figure Captions:

Figure 1: (37x67 mm + 19 = 123 words)

Chemical structures of the four C_6H_{12} isomers used in this study as a fuel for burner-stabilized flat $C_6H_{12}/O_2/Ar$ flames.

Figure 2: (52x67 mm + 26 = 162 words)

Mole fraction profiles of benzene as a function of distance from the burner in rich flames of 1-hexene (1HX), cyclohexane (CHX), methylcyclopentane (MCP), and 3,3-dimethyl-1-butene (DMB).

Figure 3: (53x67 mm + 23 = 162 words)

Maximum mole fractions of C_3H_5, C_3H_6, C_4H_6, and C_5H_6 in the fuel-rich flames of 1-hexene (1HX), cyclohexane (CHX), methylcyclopentane (MCP), and 3,3-dimethyl-1-butene (DMB).

Figure 4: (149x67 mm + 89 = 440 words)

(a) Photoionization efficiency (PIE) curves of *m/z*=42 (ketene+propene) from rich 1HX and DMB flames and PIE curves of propene and ketene. (b) PIE curves of *m/z*=54 (C_4H_6) sampled from rich 1HX, CHX, and DMB flames are reproduced accurately by contributions from 1,3-, and 1,2-butadiene and 2-butyne. (c) PIE curves of *m/z*=68 (C_5H_8) from rich DMB and MCP flames are shown. For the MCP flame, the PIE curve is reproduced by a weighted sum of contributions of 1,3-pentadiene and cyclopentene. Ionization energies of the CH_2=CH-C(CH_3)=CH_2 and CH_2=C=C(CH_3)$_2$ isomer are marked.

Figure 5: (147x67 mm + 96 = 441 words)

Correlation of benzene mole fractions to the maximum mole fractions of (a) C_3H_3, (b) C_4H_5, and (c) C_5H_5 for the four C_6H_{12} flames studied here and for several literature flame data. See text for details: acetylene (C_2H_2), ethylene (C_2H_4), propene (C_3H_6), propyne (C_3H_8), 1,3-butadiene (13B), cyclopentene (CP), 1-hexene (1HX), cyclohexane (CHX), methylcyclopentane (MCP), 3,3-dimethyl-1-butene (DMB). Open symbols represent data from flames fueled by species with a five- or six-membered ring structure; closed symbols are used for data from non-cyclic fuels. In Fig. 5(b), the marked section of the lower left corner is shown enlarged as insert.

Figure 1:

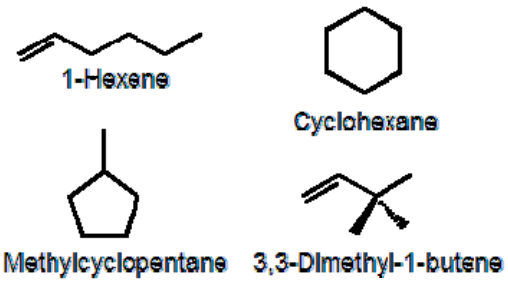
1-Hexene
Cyclohexane
Methylcyclopentane
3,3-Dimethyl-1-butene

Figure 2:

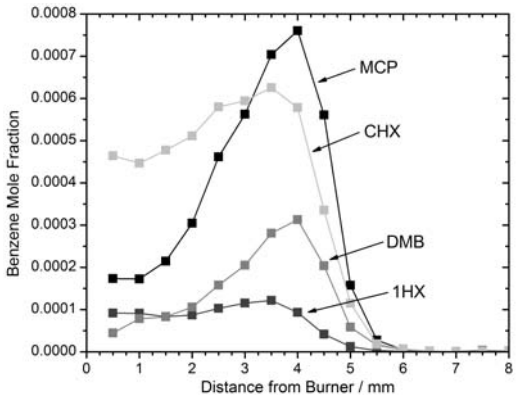
Benzene Mole Fraction
Distance from Burner / mm
MCP
CHX
DMB
1HX
0.0000
0.0001
0.0002
0.0003
0.0004
0.0005
0.0006
0.0007
0.0008
0
1
2
3
4
5
6
7
8

Figure 3:

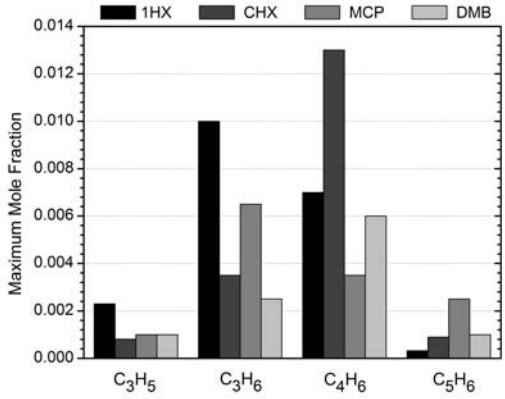
1HX
CHX
MCP
DMB
Maximum Mole Fraction
0.014
0.012
0.010
0.008
0.006
0.004
0.002
0.000
C3H5
C3H6
C4H6
C5H6

Figure 4:

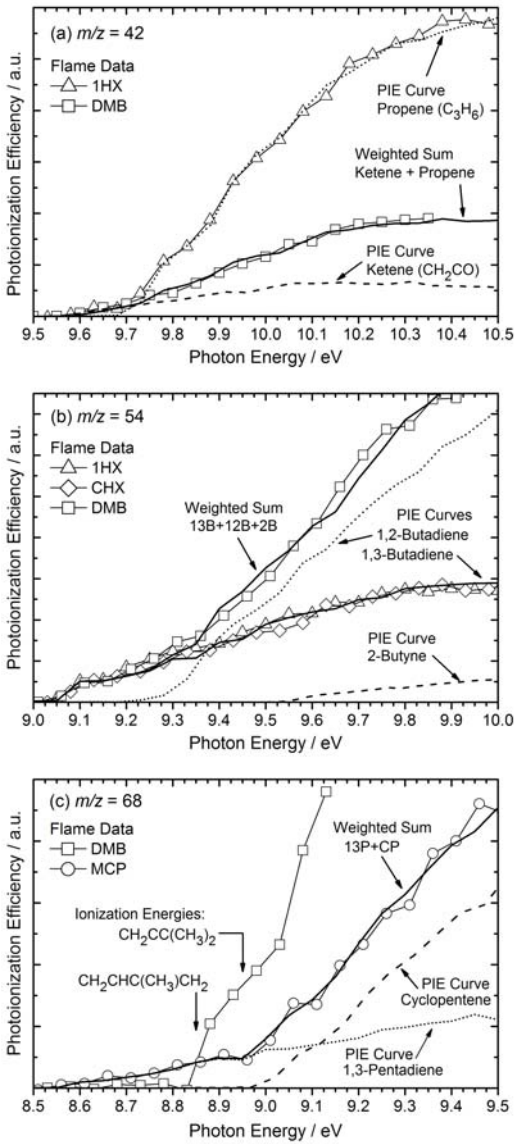
(a) m/z = 42
Flame Data
1HX
DMB
PIE Curve
Propene (C3H6)
Weighted Sum
Ketene + Propene
PIE Curve
Ketene (CH2CO)
Photoionization Efficiency / a.u.
Photon Energy / eV
(b) m/z = 54
Flame Data
1HX
CHX
DMB
Weighted Sum
13B+12B+2B
PIE Curves
1,2-Butadiene
1,3-Butadiene
PIE Curve
2-Butyne
Photoionization Efficiency / a.u.
Photon Energy / eV
(c) m/z = 68
Flame Data
DMB
MCP
Weighted Sum
13P+CP
Ionization Energies:
CH2CC(CH3)2
CH2CHC(CH3)CH2
PIE Curve
Cyclopentene
PIE Curve
1,3-Pentadiene
Photoionization Efficiency / a.u.
Photon Energy / eV

Figure 5:

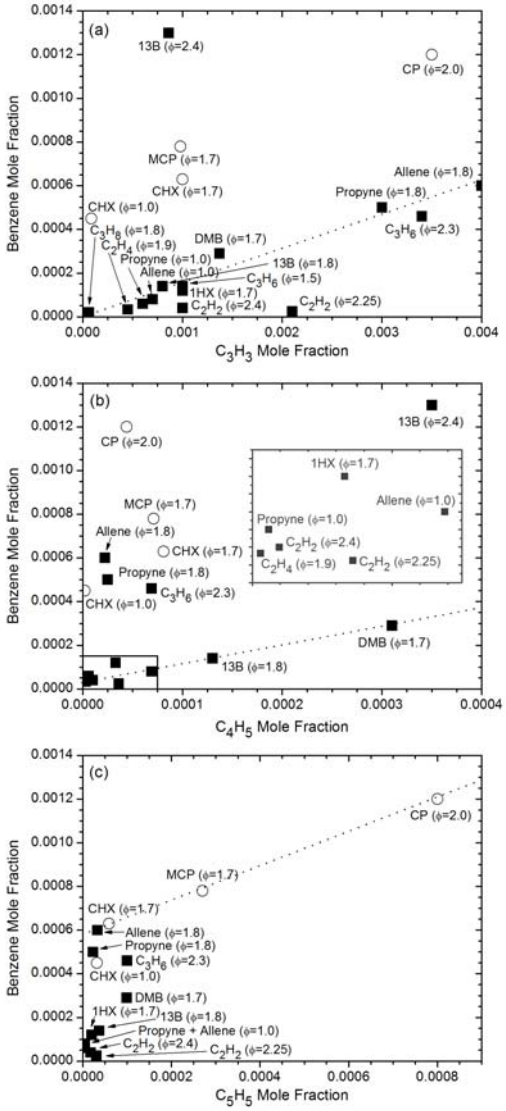
(a)
13B (ϕ=2.4)
CP (ϕ=2.0)
MCP (ϕ=1.7)
CHX (ϕ=1.7)
Allene (ϕ=1.8)
Propyne (ϕ=1.8)
CHX (ϕ=1.0)
C3H6 (ϕ=1.8)
C2H4 (ϕ=1.9)
DMB (ϕ=1.7)
C3H6 (ϕ=2.3)
Propyne (ϕ=1.0)
13B (ϕ=1.8)
Allene (ϕ=1.0)
C3H6 (ϕ=1.5)
1HX (ϕ=1.7)
C2H2 (ϕ=2.4)
C2H2 (ϕ=2.25)
Benzene Mole Fraction
C3H3 Mole Fraction
(b)
13B (ϕ=2.4)
CP (ϕ=2.0)
1HX (ϕ=1.7)
Allene (ϕ=1.0)
MCP (ϕ=1.7)
Propyne (ϕ=1.0)
Allene (ϕ=1.8)
C2H2 (ϕ=2.4)
CHX (ϕ=1.7)
C2H4 (ϕ=1.9)
C2H2 (ϕ=2.25)
Propyne (ϕ=1.8)
C3H6 (ϕ=2.3)
CHX (ϕ=1.0)
DMB (ϕ=1.7)
13B (ϕ=1.8)
Benzene Mole Fraction
C4H5 Mole Fraction
(c)
CP (ϕ=2.0)
MCP (ϕ=1.7)
CHX (ϕ=1.7)
Allene (ϕ=1.8)
Propyne (ϕ=1.8)
C3H6 (ϕ=2.3)
CHX (ϕ=1.0)
DMB (ϕ=1.7)
1HX (ϕ=1.7)
13B (ϕ=1.8)
Propyne + Allene (ϕ=1.0)
C2H2 (ϕ=2.4)
C2H2 (ϕ=2.25)
Benzene Mole Fraction
C5H5 Mole Fraction